Hierarchical mesoporous perovskite $La_{0.5}Sr_{0.5}CoO_{2.91}$ nanowires with ultrahigh capacity for Li-air batteries

Yunlong Zhao[1], Lin Xu[1], Liqiang Mai[2], Chunhua Han, Qinyou An, Xu Xu, Xue Liu, and Qingjie Zhang

State Key Laboratory of Advanced Technology for Materials Synthesis and Processing, Wuhan University of Technology, Wuhan 430070, China

Edited* by Charles M. Lieber, Harvard University, Cambridge, MA, and approved October 10, 2012 (received for review June 18, 2012)

Lithium-air batteries have captured worldwide attention due to their highest energy density among the chemical batteries. To provide continuous oxygen channels, here, we synthesized hierarchical mesoporous perovskite $La_{0.5}Sr_{0.5}CoO_{2.91}$ (LSCO) nanowires. We tested the intrinsic oxygen reduction reaction (ORR) and oxygen evolution reaction (OER) activity in both aqueous electrolytes and nonaqueous electrolytes via rotating disk electrode (RDE) measurements and demonstrated that the hierarchical mesoporous LSCO nanowires are high-performance catalysts for the ORR with low peak-up potential and high limiting diffusion current. Furthermore, we fabricated Li-air batteries on the basis of hierarchical mesoporous LSCO nanowires and nonaqueous electrolytes, which exhibited ultrahigh capacity, ca. over 11,000 mAh·g^{-1}, one order of magnitude higher than that of LSCO nanoparticles. Besides, the possible reaction mechanism is proposed to explain the catalytic activity of the LSCO mesoporous nanowire.

electrocatalysis | energy storage

W

Author contributions: Y.Z. and L.M. designed research; Y.Z. and X.L. performed research; Y.Z. and L.X. contributed new reagents/analytic tools; Y.Z., L.X., C.H., Q.A., X.X., and Q.Z. analyzed data; and Y.Z., L.X., and L.M. wrote the paper.

The authors declare no conflict of interest.

*This Direct Submission article had a prearranged editor.

[1]Y.Z. and L.X. contributed equally to this work.

[2]To whom correspondence

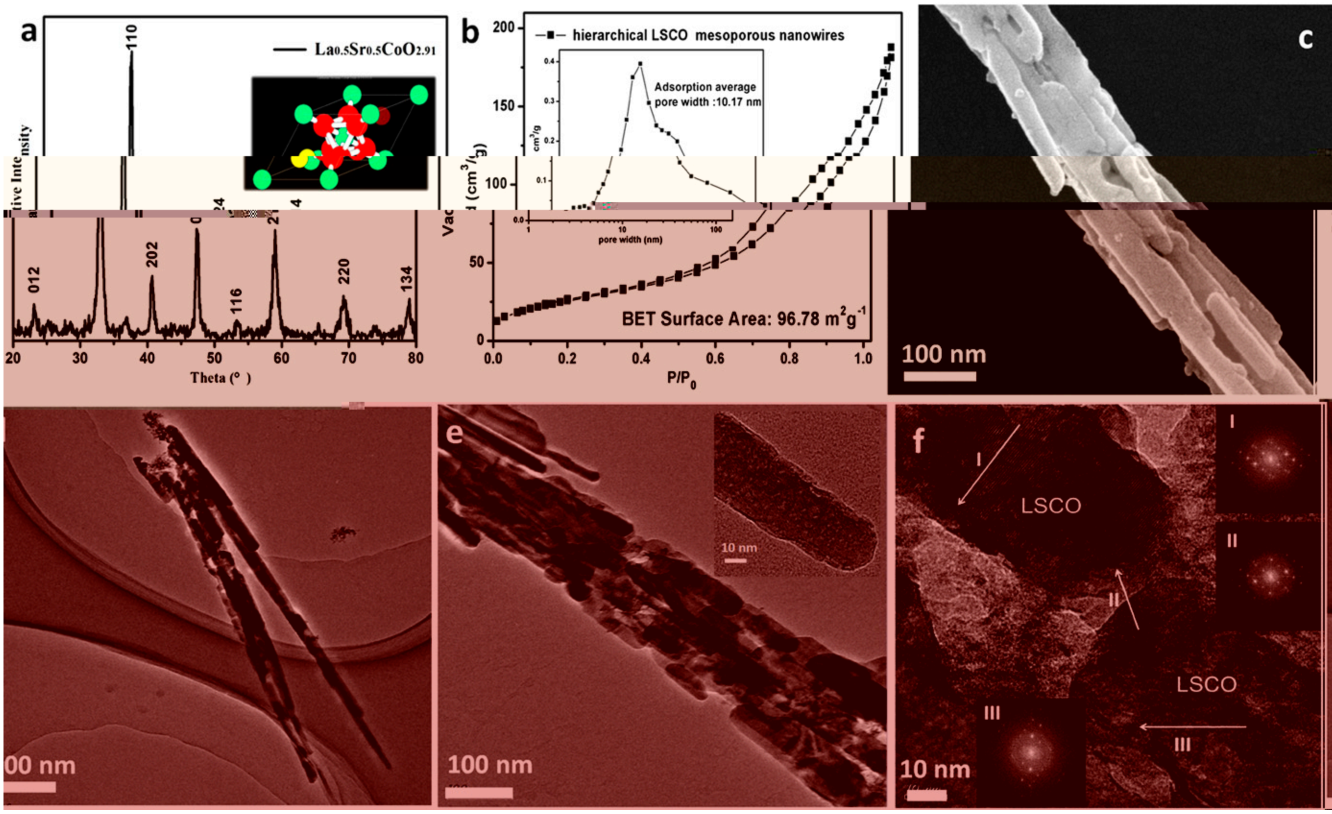

Fig. 1. Phase analysis and morphology characterization. (*A*) XRD pattern of hierarchical mesoporous LSCO nanowires after annealing. (*Inset* shows a model of the perovskite structure LSCO. Green balls represent Co atoms; red balls, O atoms; yellow ball, a La atom; and wine ball, a Sr atom. One of the apical oxygen sites is vacated and the unit cell is doubled.) (*B*) Nitrogen adsorption and desorption isotherms and pore size distribution (*Inset*) of hierarchical mesoporous LSCO nanowires after annealing. (*C*) SEM image of the hierarchical mesoporous LSCO nanowires. (*D* and *E*) TEM and HRTEM images of the hierarchical mesoporous LSCO nanowires (*Inset* shows porous LSCO nanorods from mesoporous nanowires). (*F*) HRTEM image at the junction of mesoporous LSCO nanowires and FFT patterns on selected areas. The arrows represent crystal lattice direction.

(Fig. 1*F*) … Fig. 1*B*. … ~10.1 … (Fig. 2).

Results and Discussion

(22, –).

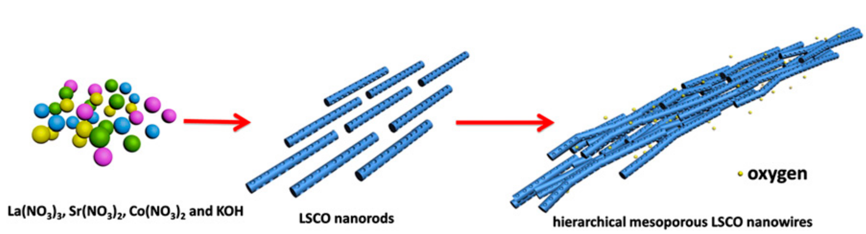

Fig. 2. The schematic model diagram of constructing hierarchical mesoporous LSCO nanowires.

$$\frac{1}{i}=\frac{1}{i_k}+\frac{1}{i_d}=\frac{1}{nFAkC}-\frac{1}{0.\ 2nFAD_2^{2/}\nu^{-1/}C\ \omega^{1/2}},\qquad [1]$$

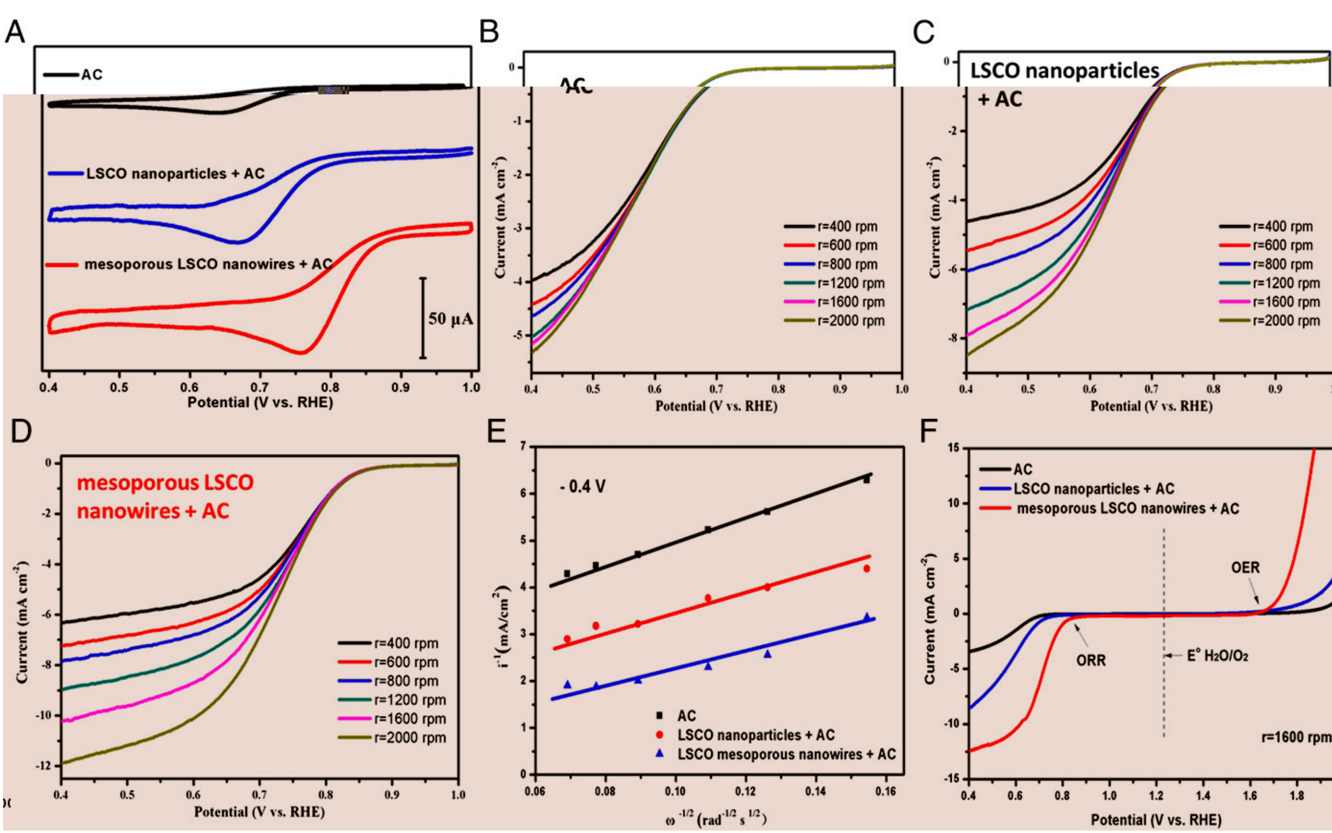

Fig. 3. Oxygen reduction and oxygen evolution catalytic performance on glassy carbon electrodes in O_2 saturated in aqueous electrolyte, 0.1 M KOH with a sweep rate of 5 $mV \cdot s^{-1}$. (*A*) CV curves of activated carbon (AC), LSCO nanoparticles + AC, and hierarchical mesoporous LSCO nanowires + AC. (*B*–*D*) ORR polarization curves of AC, LSCO nanoparticles + AC, and hierarchical mesoporous LSCO nanowires + AC at different rotation rates. (*E*) Koutecky–Levich plot based on ORR polarization curves at −0.4 V. (*F*) ORR and OER polarization curves of AC, LSCO nanoparticles + AC, and hierarchical mesoporous LSCO nanowires + AC on glassy carbon electrodes at 1,600-rpm rotation rates.

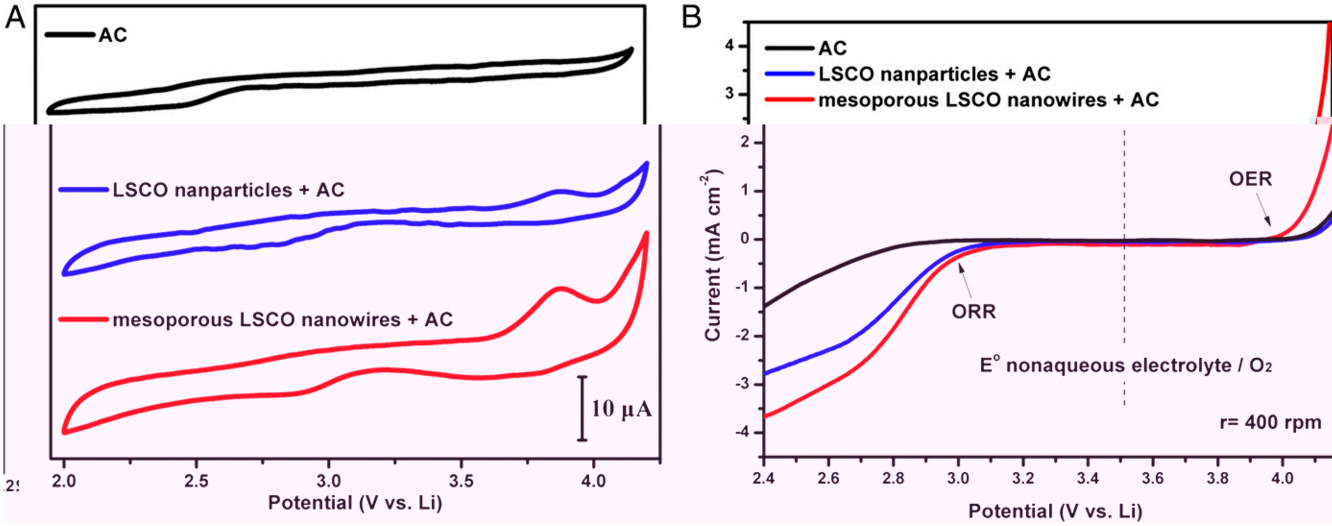

Fig. 4. Oxygen reduction and oxygen evolution catalytic performance on glassy carbon electrodes in O_2 saturated in nonaqueous electrolyte with a sweep rate of 5 mV·s^{-1}. Lithium metal was used as a counterelectrode. (*A*) CV curves of AC, LSCO nanoparticles + AC, and hierarchical mesoporous LSCO nanowires + AC. (*B*) ORR and OER polarization curves of AC, LSCO nanoparticles + AC, and hierarchical mesoporous LSCO nanowires + AC on glassy carbon electrodes at 400-rpm rotation rates.

B B , B 2.0 . A. B B B
B , B B 2 B B S +
(. S *A*). B B - , 2 / . , B B
fi - B B B , . *B–D*. S ,
(B B B S +
B 1) . B 0 B B B 11,0 /
/ , B S 2 2. B B ffB 2 , / ,
.2 . B B B B B 2. . B B S
B / B B - + B ffB B -
B B B , B B B (1, /) S B + (, 02

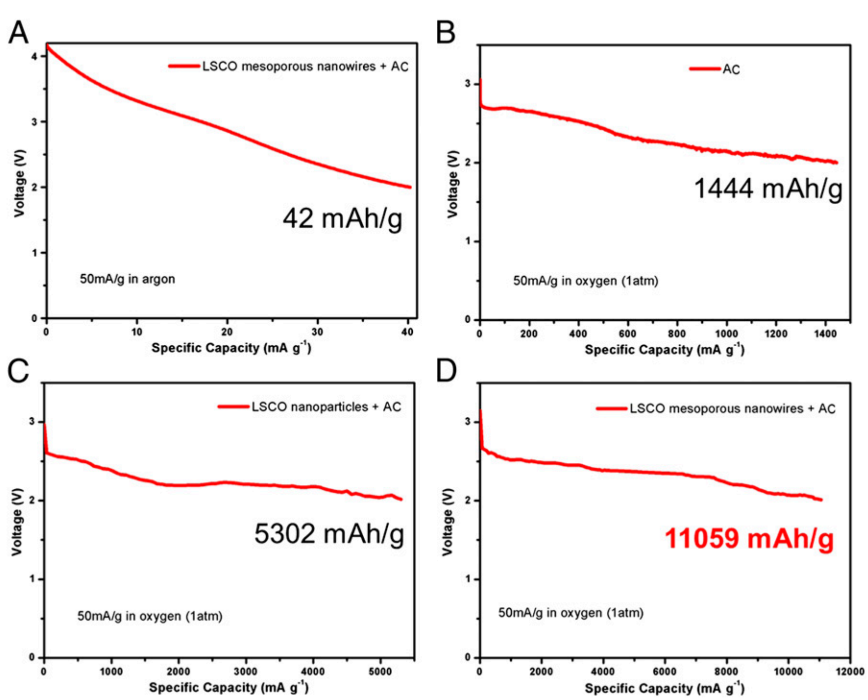

Fig. 5. Electrochemical performances of Li-air batteries. (*A*) The discharge curve of Li-air batteries using hierarchical mesoporous LSCO nanowires + AC as the air electrode in the pure argon atmosphere. (*B–D*) The discharge curve of Li-air batteries using AC, LSCO nanoparticles + AC, and hierarchical mesoporous LSCO nanowires + AC as the air electrode in oxygen (Po_2 = 1 atm).

Materials and Methods

Materials Synthesis. Hierarchical mesoporous perovskite LSCO nanowires were synthesized using a facile multistep microemulsion with $La(NO_3)_3$, $Sr(NO_3)_2$, $Co(NO_3)_2$, and KOH, which was followed by vigorous stirring and then slow stirring for 6 h at room temperature and aging for 24 h after demulsification. The nanowires were then annealed at 800 °C at the rate of 1 °C/min in argon gas to obtain hierarchical perovskite $La_{0.5}Sr_{0.5}CoO_{2.91}$ mesoporous nanowires. As a control experiment, LSCO nanoparticles were also synthesized by a similar proportion but rapid annealing was used (10 °C/min) (synthesis details in Fig. S1).

Electrochemical Measurements. Five milligrams of AC (XC-72) or 0.75 mg of LSCO nanoparticles mixed with 4.25 mg of AC or 0.75 mg hierarchical mesoporous LSCO nanowires mixed with 4.25 mg AC and 122 μL of 5 wt% Nafion solutions were dispersed in 1 mL of 3:1 vol/vol water/isopropanol mixed solvent by at least 30 min sonication to form a homogeneous ink. A saturated calomel electrode was used as the reference electrode in all measurements and was calibrated with respect to a reversible hydrogen electrode. Cyclic voltammetry and linear scanning voltammetry were conducted in a three-electrode electrochemical cell. Twenty micrograms of sample was loaded on the glassy carbon working electrode (5 mm in diameter). Electrochemical data were collected with an Autolab electrochemical workstation. KOH (0.1 M) and $LiPF_6$ (1 M) in ethylene carbon/dimethyl carbonate were used as the electrolyte. The three-electrode cell used for RDE measurements (Pine) consists of a platinum electrode as a counterelectrode, a saturated calomel electrode as a reference electrode or a lithium-foil counterelectrode, and a platinum electrode as a reference electrode. For the measurement on filter paper, the working electrode was prepared by loading 2 mg of sample from its ink. The electrochemical properties were carried out by assembling 2,025 coin cells in a glove box filled with pure argon gas, using a lithium pellet as the anode, 1 M solution of $LiPF_6$ in ethylene carbon (EC)/dimethyl carbonate (DMC) as the electrolyte, and filter paper-supported samples as cathode electrodes. Galvanostatic discharge was studied in a potential range of 4.2–2.0 V vs. Li/Li^+ with a multichannel battery testing system (LAND CT 2001A).

Characterization. The crystal phase and purity of the products were characterized by X-ray powder diffraction. X-ray diffraction patterns of the products were recorded on a Rigaku D/MAX-III diffractometer with monochromatized Cu K_a radiation (k = 1.5406 Å). Field-emission scanning electron microscopy images were collected with a Hitachi S-4800 at an acceleration voltage of 10 kV. TEM and HRTEM images were recorded by using a JEOL JEM-2010 FEF microscope at an accelerating voltage of 200 kV. Energy dispersive spectroscopy (EDS) was performed on a JEM 2100F STEM/EDS. Nitrogen adsorption and desorption isotherms were measured using a Gemini 2360 instrument by adsorption of nitrogen at −209 °C.

ACKNOWLEDGMENTS. This work was supported by the National Basic Research Program of China (2013CB934103, 2012CB933003), the National Natural Science Foundation of China (51272197 and 51072153), the International S&T Cooperation (2013ZR02930), the Program for New Century Excellent Talents in University (NCET-10-0661), and the Fundamental Research Funds for the Central Universities (2011-II-012).

1. Armand M, Tarascon JM (2008) Building better batteries. *Nature* 451(7179):652–657.
2. Dunn B, Kamath H, Tarascon JM (2011) Electrical energy storage for the grid: A battery of choices. *Science* 334(6058):928–935.
3. Bruce PG, Scrosati B, Tarascon JM (2008) Nanomaterials for rechargeable lithium batteries. *Angew Chem Int Ed Engl* 47(16):2930–2946.
4. Mai LQ, et al. (2011) Hierarchical $MnMoO_{(4)}/CoMoO_{(4)}$ heterostructured nanowires with enhanced supercapacitor performance. *Nat Commun* 2:381.
5. Tian B, Kempa TJ, Lieber CM (2009) Single nanowire photovoltaics. *Chem Soc Rev* 38 (1):16–24.
6. Kempa TJ, et al. (2012) Coaxial multishell nanowires with high-quality electronic interfaces and tunable optical cavities for ultrathin photovoltaics. *Proc Natl Acad Sci USA* 109(5):1407–1412.
7. Goodenough JB, Kim Y (2009) Challenges for rechargeable Li batteries. *Chem Mater* 22:587–603.
8. Tarascon JM, Armand M (2001) Issues and challenges facing rechargeable lithium batteries. *Nature* 414(6861):359–367.
9. Abraham K, Jiang Z (1996) A Polymer electrolyte-based rechargeable lithium/oxygen battery. *J Electrochem Soc* 143:1–5.
10. Bruce PG, Freunberger SA, Hardwick LJ, Tarascon JM (2012) Li-O_2 and Li-S batteries with high energy storage. *Nat Mater* 11(1):19–29.
11. Cui Y, Wen Z, Liu Y (2011) A free-standing-type design for cathodes of rechargeable Li-O_2 batteries. *Energy Environ Sci* 4:4727–4734.
12. Suntivich J, et al. (2011) Design principles for oxygen-reduction activity on perovskite oxide catalysts for fuel cells and metal-air batteries. *Nat Chem* 3(7):546–550.
13. Kraytsberg A, Ein-Eli Y (2011) Review on Li-air batteries-opportunities, limitations and perspective. *J Power Sources* 196:886–893.
14. Jung HG, Hassoun J, Park JB, Sun YK, Scrosati B (2012) An improved high-performance lithium-air battery. *Nat Chem* 4(7):579–585.
15. Peng Z, Freunberger SA, Chen Y, Bruce PG (2012) A reversible and higher-rate Li-O_2 battery. *Science* 337(6094):563–566.
16. Lu YC, et al. (2010) Platinum-gold nanoparticles: A highly active bifunctional electrocatalyst for rechargeable lithium-air batteries. *J Am Chem Soc* 132(35): 12170–12171.
17. Veith GM, Dudney NJ (2011) Current collectors for rechargeable Li-air batteries. *J Electrochem Soc* 158:A658–A663.
18. Xiao J, et al. (2011) Hierarchically porous graphene as a lithium-air battery electrode. *Nano Lett* 11(11):5071–5078.
19. Freunberger SA, et al. (2011) Reactions in the rechargeable lithium-O_2 battery with alkyl carbonate electrolytes. *J Am Chem Soc* 133(20):8040–8047.
20. Xiao J, et al. (2010) Optimization of air electrode for Li/air batteries. *J Electrochem Soc* 157:A487–A492.
21. Suntivich J, May KJ, Gasteiger HA, Goodenough JB, Shao-Horn Y (2011) A perovskite oxide optimized for oxygen evolution catalysis from molecular orbital principles. *Science* 334(6061):1383–1385.
22. Suntivich J, Gasteiger HA, Yabuuchi N, Shao-Horn Y (2010) Electrocatalytic measurement methodology of oxide catalysts using a thin-film rotating disk electrode. *J Electrochem Soc* 157:B1263–B1268.
23. Mirzaeian M, Hall PJ (2009) Preparation of controlled porosity carbon aerogels for energy storage in rechargeable lithium oxygen batteries. *Electrochim Acta* 54: 7444–7451.
24. Wu Z, Lv Y, Xia Y, Webley PA, Zhao D (2012) Ordered mesoporous platinum@-graphitic carbon embedded nanophase as a highly active, stable, and methanol-tolerant oxygen reduction electrocatalyst. *J Am Chem Soc* 134(4):2236–2245.
25. Zhou L, Zhao D, Lou XW (2012) Double-shelled $CoMn_2O_4$ hollow microcubes as high-capacity anodes for lithium-ion batteries. *Adv Mater (Deerfield Beach Fla)* 24(6): 745–748.
26. Mai LQ, et al. (2010) Electrospun ultralong hierarchical vanadium oxide nanowires with high performance for lithium ion batteries. *Nano Lett* 10(11):4750–4755.
27. Deng J, Zhang L, Dai H, He H, Au CT (2008) Single-crystalline $La_{0.6}Sr_{0.4}CoO_{3-\delta}$ nanowires/nanorods derived hydrothermally without the use of a template: Catalysts highly active for toluene complete oxidation. *Catal Lett* 123:294–300.
28. Donner W, et al. (2011) Epitaxial strain-induced chemical ordering in $La_{0.5}Sr_{0.5}CoO_{3-\delta}$ films on $SrTiO_3$. *Chem Mater* 23:984–988.
29. Li WW, et al. (2010) Growth, microstructure, and infrared-ultraviolet optical conductivity of $La_{(0.5)}Sr_{(0.5)}CoO_{(3)}$ nanocrystalline films on silicon substrates by pulsed laser deposition. *ACS Appl Mater Interfaces* 2(3):896–902.
30. Liu W, et al. (2008) $La_{0.5}Sr_{0.5}CoO_{3-\delta}$ nanotubes sensor for room temperature detection of ammonia. *Sens Actuators B Chem* 134:62–65.
31. Yu HC, Fung KZ, Guo TC, Chang WL (2004) Syntheses of perovskite oxides nanoparticles $La_{1-x}Sr_xMO_{3-\delta}$ (M = Co and Cu) as anode electrocatalyst for direct methanol fuel cell. *Electrochim Acta* 50(2–3):811–816.
32. Wang Y, Fan HJ (2010) Improved thermoelectric properties of $La_{1-x}Sr_xCoO_3$ nanowires. *J Phys Chem C* 114:13947–13953.
33. Byon HR, Suntivich J, Shao-Horn Y (2011) Graphene-based non-noble-metal catalysts for oxygen reduction reaction in acid. *Chem Mater* 23:3421–3428.
34. Cheng F, Su Y, Liang J, Tao Z, Chen J (2009) MnO_2-based nanostructures as catalysts for electrochemical oxygen reduction in alkaline media. *Chem Mater* 22:898–905.
35. Débart A, Bao J, Armstrong G, Bruce PG (2007) An O_2 cathode for rechargeable lithium batteries: The effect of a catalyst. *J Power Sources* 174:1177–1182.
36. Liang Y, et al. (2011) Co_3O_4 nanocrystals on graphene as a synergistic catalyst for oxygen reduction reaction. *Nat Mater* 10(10):780–786.
37. Lim B, et al. (2009) Pd-Pt bimetallic nanodendrites with high activity for oxygen reduction. *Science* 324(5932):1302–1305.
38. Lu YC, Gasteiger HA, Parent MC, Chiloyan V, Shao-Horn Y (2010) The influence of catalysts on discharge and charge voltages of rechargeable Li–oxygen batteries. *Electrochem Solid-State Lett* 13:A69–A72.
39. Lu YC, Gasteiger HA, Shao-Horn Y (2011) Method development to evaluate the oxygen reduction activity of high-surface-area catalysts for Li-air batteries. *Electrochem Solid-State Lett* 14:A70–A74.
40. Lu YC, Gasteiger HA, Shao-Horn Y (2011) Catalytic activity trends of oxygen reduction reaction for nonaqueous Li-air batteries. *J Am Chem Soc* 133(47):19048–19051.
41. Yin F, Takanabe K, Katayama M, Kubota J, Domen K (2010) Improved catalytic performance of nitrided Co-Ti and Fe-Ti catalysts for oxygen reduction as non-noble metal cathodes in acidic media. *Electrochem Commun* 12:1177–1179.
42. Cheng F, et al. (2011) Rapid room-temperature synthesis of nanocrystalline spinels as oxygen reduction and evolution electrocatalysts. *Nat Chem* 3(1):79–84.
43. Wang L, et al. (2011) $CoMn_2O_4$ spinel nanoparticles grown on graphene as bifunctional catalyst for lithium-air batteries. *J Electrochem Soc* 158:A1379–A1382.